Inorganic Chemistry

pubs.acs.org/IC Article

"Half-Sandwich" Ruthenium Complexes with Alizarin as Anticancer Agents: *In Vitro* and *In Vivo* Studies

João Honorato de Araujo-Neto,* Adriana P. M. Guedes, Celisnolia M. Leite, Carlos André F. Moraes, Andressa L. Santos, Rafaella da S. Brito, Thiago L. Rocha, Francyelli Mello-Andrade, Javier Ellena, and Alzir A. Batista*

Cite This: *Inorg. Chem.* 2023, 62, 6955−6969 Read Online

ACCESS | Metrics & More | Article Recommendations | Supporting Information

ABSTRACT: Upon exploration of the chemistry of the combination of ruthenium/arene with anthraquinone alizarin (L), three new complexes with the general formulas [Ru(L)Cl(η^6-*p*-cymene)] (**C1**), [Ru(L)(η^6-*p*-cymene)(PPh_3)]PF_6 (**C2**), and [Ru(L)(η^6-*p*-cymene)(PEt_3)]PF_6 (**C3**) were synthesized and characterized using spectroscopic techniques (mass, IR, and 1D and 2D NMR), molar conductivity, elemental analysis, and X-ray diffraction. Complex **C1** exhibited fluorescence, such as free alizarin, while in **C2** and **C3**, the emission was probably quenched by monophosphines and the crystallographic data showed that hydrophobic interactions are predominant in intermolecular contacts. The cytotoxicity of the complexes was evaluated in the MDA-MB-231 (triple-negative breast cancer), MCF-7 (breast cancer), and A549 (lung) tumor cell lines and MCF-10A (breast) and MRC-5 (lung) nontumor cell lines. Complexes **C1** and **C2** were more selective to the breast tumor cell lines, and **C2** was the most cytotoxic (IC_{50} = 6.5 μM for MDA-MB-231). In addition, compound **C1** performs a covalent interaction with DNA, while **C2** and **C3** present only weak interactions; however, internalization studies by flow cytometry and confocal microscopy showed that complex **C1** does not accumulate in viable MDA-MB-231 cells and is detected in the cytoplasm only after cell permeabilization. Investigations of the mechanism of action of the complexes indicate that **C2** promotes cell cycle arrest in the Sub-G_1 phase in MDA-MB-231, inhibits its colony formation, and has a possible antimetastatic action, impeding cell migration in the wound-healing experiment (13% of wound healing in 24 h). The *in vivo* toxicological experiments with zebrafish indicate that **C1** and **C3** exhibit the most zebrafish embryo developmental toxicity (inhibition of spontaneous movements and heartbeats), while **C2**, the most promising anticancer drug in the *in vitro* preclinical tests, revealed the lowest toxicity in *in vivo* preclinical screening.

INTRODUCTION

The search for new and necessary alternatives for the treatment of different types of diseases is one of the researchers' main tasks from different areas of knowledge. Among these diseases, cancer is one of the most prominent because it caused about 10 million deaths in 2020.[1] In this context, the investigation of new, more efficient, and cheaper alternatives for cancer treatment, such as new drugs for chemotherapy, or inclusive new forms of treatment has provided hope for an attempt to mitigate the effects of the pandemic or other causes and reduce the number of deaths caused by cancer. Thus, one prominent and promising drug candidate class is the "half-sandwich" ruthenium/arene compounds, mainly due to the emphasis received by the compound [Ru(η^6-*p*-cymene)Cl_2PTA] (PTA = 1,3,5-triaza-7-phosphaadamantane), called RAPTA-C.[2] Different from other metal complexes that tend to bind to DNA, RAPTA-C tends to be more interactive toward proteins, focusing on different targets in the cell and consequently different modes of action.[3] This complex appears to be a promising candidate to reach clinical evaluation, exhibiting anticancer efficacy, as demonstrated by experiments *in vitro* as well as *in vivo*, leading to, for instance, a 50% reduction of the number of lung metastases in mice.[4−6] Furthermore, RAPTA-C can perform the blockage of T-cell-associated proteins, enabling experimentation of this compound as an immunotherapeutic drug.[7,8]

The potency demonstrated by the RAPTA complexes has led to the exploration of several other structural combinations, aiming to use (in this system) different ligands that would trigger other modes of interaction with different biomolecular targets. Among these structures, we can highlight complexes containing bidentate ligands that coordinate to the metallic center through O,O-coordinating ligands.[9] These combinations resulted in the obtainment of metal chelates with four-, five-, or six-membered chelate rings with different classes of

Received: January 16, 2023
Published: April 26, 2023

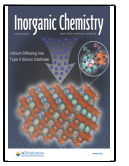

https://doi.org/10.1021/acs.inorgchem.3c00183
Inorg. Chem. 2023, 62, 6955−6969

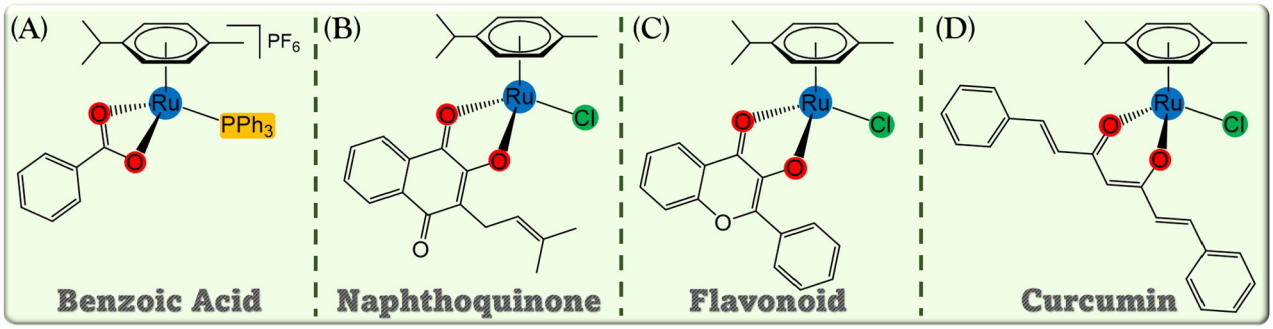

Figure 1. Examples of ruthenium/arene complexes with O,O-coordinating ligands such as benzoic acid and analogues,[10] naphthoquinones,[11,20] flavonoids,[13] and curcumins.[19]

Scheme 1. Synthesis of the Ruthenium(II)/Arene/Alizarin Complexes

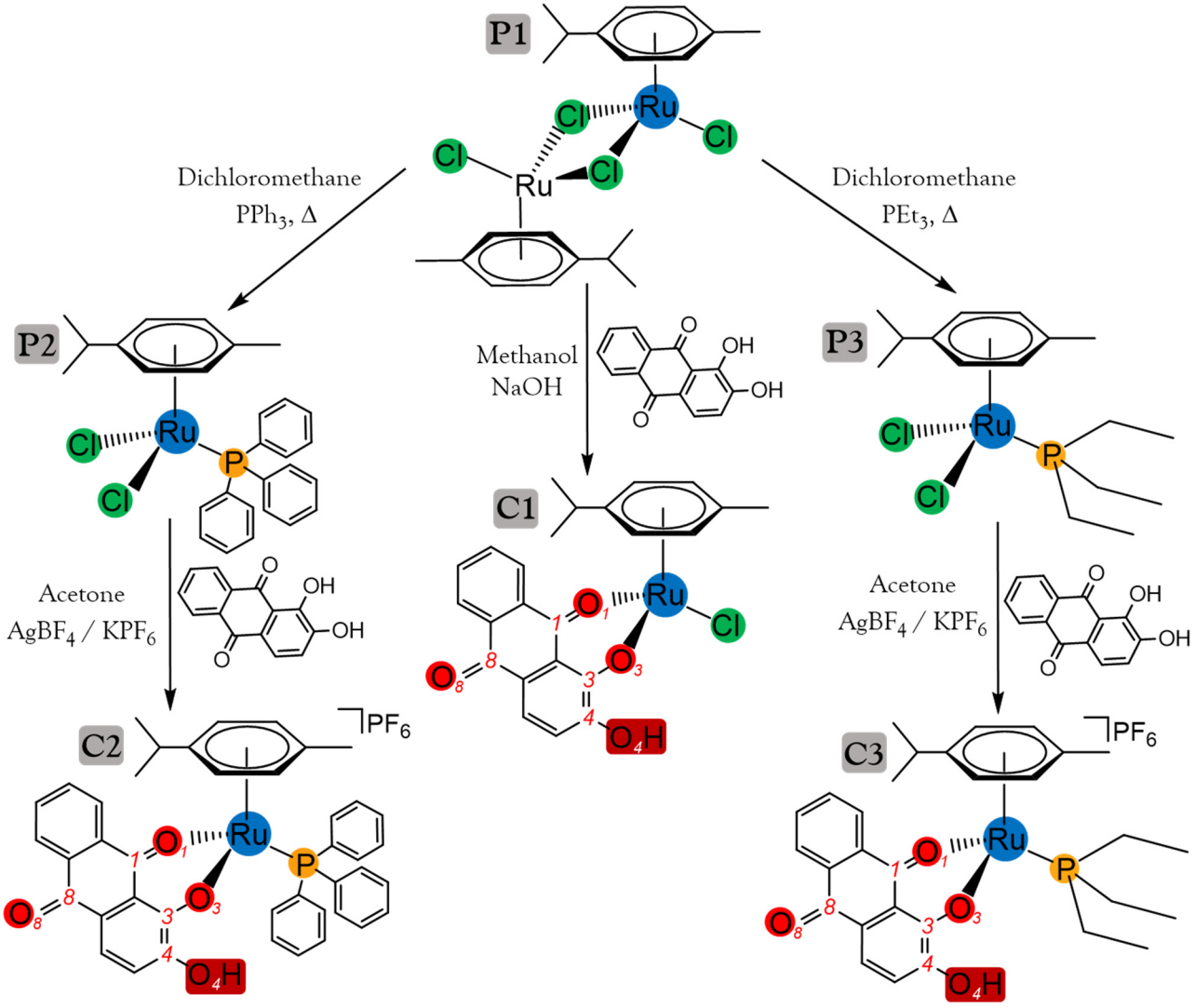

organic molecules, as exemplified in Figure 1A. Our research group has already explored the chemistry of "half-sandwich" ruthenium/arene compounds containing benzoic acid and analogues as ligands (four-membered chelate ring), resulting in complexes that are selective for breast cancer cells (MDA-MB-231) and capable of accumulating in tumor cells.[10] Natural products, such as naphthoquinones (Figure 1B) and flavonoids (Figure 1C), have also been coordinated to ruthenium/arene complexes, resulting in five-membered chelate rings. These complexes containing lapachol (naphthoquinone) display *in vitro* anticancer activity, whose mechanism involves the generation of reactive oxygen species and consequent oxidative stress. The ruthenium/arene/flavonoid complexes trigger cell death mechanisms by topoisomerase IIα inhibition and covalent DNA binding.[11−15] Another powerful combination with natural products is complexes containing curcumins

https://doi.org/10.1021/acs.inorgchem.3c00183
Inorg. Chem. 2023, 62, 6955−6969

Table 1. Carbonyl IR Stretching and NMR Chemical Shift Values for Complexes C1−C3 and Free Alizarin and Fluorescence Quantum Yield of Complexes C1−C3 (TPyP as a Standard)

	IR		^{13}C NMR				
	$\nu(C_1{=}O_1)$ (cm^{-1})	$\nu(C_8{=}O_8)$ (cm^{-1})	$\delta(C_1{=}O_1)$ (ppm)	$\delta(C_3{-}O_3)$ (ppm)	$\delta(C_4{-}O_4)$ (ppm)	$\delta(C_8{=}O_8)$ (ppm)	fluorescence quantum yield (%)
C1	1610	1660	182.2	155.9	158.4	181.2	12.0
C2	1610	1656	182.2	157.2	157.2	180.5	0.5
C3	1612	1651	184.5	158.5	156.6	180.5	0.9
alizarin	1633	1664	181.5	151.0	149.3	189.5	16.2

(Figure 1D), resulting in the formation of six-membered chelate rings and high inhibition of the proliferation of breast and ovarian tumor cells and also covalently binding to DNA (Ru/N_7-guanine) and suppressing the proteasome activity.[16−19]

An underexplored class of ligands that can form six-membered chelated rings, as those described above, is anthraquinones, such as alizarin, which can be found in the roots of *Rubia tinctorum* and is used as a fluorescent organic red dye.[21] Studies on the antitumor action of alizarin reported that this molecule exhibits an inhibitory effect on cells derived from human colon carcinoma[22] and osteosarcoma.[23] An important characteristic exhibited by alizarin is the absence of stimulation of cell proliferation, mutagenicity, or malignant transformation,[24,25] showing no tumor-promoting activity, making this molecule an interesting ligand for the synthesis of new complexes.

Zebrafish (*Danio rerio*) is an appropriate animal preclinical model system for *in vivo* toxicological screening drugs for potential use in the treatment of human diseases, such as cancer.[26] In addition, zebrafish has been an experimental model widely adopted in scientific research in several areas, including pharmacology and toxicology.[27,28] Some key features that make it an excellent model for use in toxicology include external fertilization, rapid development, high reproduction rate, the possibility of assessing early development due to chorion translucency, genome already sequenced, and high homology with humans.[29−31] The zebrafish model system has been recommended and adopted for toxicological preclinical screening to reduce the time and cost of the drug discovery process[32−34] as an alternative model based on 10Rs ethical principles.[35]

Accordingly, the current study aimed to evaluate the antitumoral (*in vitro*) and toxicological safety (*in vivo*) characteristics of new "half-sandwich" ruthenium/alizarin complexes, using breast and lung cancer cells, investigating the DNA interaction and *in vitro* antimetastatic effect of these complexes. In a complementary way, we will check the toxicological safety using the zebrafish model associated with a multiple biomarker response, such as the mortality rate, hatching rate, morphological change, neurotoxicity, and cardiotoxicity, aiming to explore the potential of these complexes as anticancer metallodrugs.

RESULTS AND DISCUSSION

Synthesis and Characterization. Complexes **C1−C3** were synthesized following the procedure shown in Scheme 1. Starting from the binuclear complex [{RuCl(η^6-*p*-cymene)}$_2$(μ-Cl)$_2$] (**P1**),[36] the mononuclear precursors [$RuCl_2$(η^6-*p*-cymene)(PPh_3)] (**P2**) and [$RuCl_2$(η^6-*p*-cymene)(PEt_3)] (**P3**) were obtained.[37−39]

To obtain [Ru(L)Cl(η^6-*p*-cymene)] (**C1**; CCDC 2161723), the neutral complex **P1** was dissolved in methanol, in the presence of the unprotonated alizarin (1:2 ratio, **P1**/L, L = alizarin), which results in a dark-blue precipitate **C1** powder. Using this same procedure, but using **P2** and **P3** as precursors in an attempt to synthesize the monocationic [Ru(L)(η^6-*p*-cymene)(PPh_3)]PF_6 (**C2**) and [Ru(L)(η^6-*p*-cymene)(PEt_3)]-PF_6 (**C3**; CCDC 2161724), the reactions reach equilibrium, not consuming all precursors, even with the presence of the counterion (PF_6^-), and reflux. Therefore, to obtain pure **C2** and **C3** complexes, the chlorido ligands were extracted by adding a silver salt ($AgBF_4$), resulting in the instant formation of AgCl precipitate and consequent coordination of alizarin to ruthenium, resulting in pure **C2** or **C3** complexes, in high yield (>95%). Previous studies carried out by our research group adopted this same method for the coordination of bidentate O−O binders to Ru^{II}.[10,40]

Elemental analysis (C, N, H, and S %) of complexes **C1−C3** agreed with their suggested structures, as in Scheme 1, and the molar conductivity, in dichloromethane, was close to 60.0 S m^2 mol^{-1} for **C2** and **C3**, which is compatible with monocationic species. Compound **C1** did not exhibit conductivity, confirming the neutrality of this complex. In the mass spectrometry experiments, the signals of the main molecular ion $[M]^+$ were observed for **C2** and **C3**, while for **C1**, the main signal was observed for the complex without the chloride ligand $[M - Cl]^+$, as presented in Figure S1A. The IR spectra of free alizarin displayed a broad band around 3400 cm^{-1}, assigned to ν(O−H), which decreases considerably its energy after its coordination to the metal center, forming the $C_1{-}O_1$ binding, leaving only $C_4{-}O_4$ in the protonated form (Figure S1B). The two ν(C=O) bands of free alizarin appeared at 1664 cm^{-1} [$\nu(C_8{=}O_8)$] and 1633 cm^{-1} [$\nu(C_1{=}O_1)$], as presented in Table 1.[41] For the three complexes, the band of $\nu(C_8{=}O_8)$ undergoes little change (around 1660 cm^{-1}), while the band of $\nu(C_1{=}O_1)$ shifts approximately 20 cm^{-1}, appearing around 1610 cm^{-1}. The decrease in the frequency of $\nu(C_1{=}O_1)$ indicates an increase in its single-bond character because of its coordination to the metal center.

C2 and **C3** formation was followed by the $^{31}P\{^1H\}$ NMR technique using aliquots of the reaction media. As usual, the unique P atom of the coordinated monophosphine ligand exhibits just one singlet signal in the NMR spectrum (CH_2Cl_2/D_2O) for both precursors and the final complexes (Figure S2). Complex **P2** exhibits this singlet signal at δ 24.2 ppm, while for **P3**, it is at δ 22.5 ppm, showing a **P2** higher chemical shift as a consequence of the π acidity of PPh_3.

All of the complexes were characterized by 1D/2D ^{1}H and ^{13}C NMR spectroscopy, with the 1D ^{1}H NMR spectra showing the same profile, with three peak regions: the first region, at high field, corresponds to the methyl/propyl H atoms (δ 1.0−3.0 ppm) of coordinated *p*-cymene and the ethyl groups from

https://doi.org/10.1021/acs.inorgchem.3c00183
Inorg. Chem. 2023, 62, 6955−6969

PEt_3 for **C3**. The second region is related to the aromatic H atoms from the coordinated *p*-cymene (δ 5.0−6.0 ppm). The third region, at low field, shows aromatic H atoms from the PPh_3 ligand for **C2** and from the alizarin ligand for all final products (δ 6.5−9.0 ppm). All registered 1D/2D spectra are presented in Figures S3−S17.

Aiming to explore the fluorescence from the coordinated alizarin molecule, in the final products, the emissive characteristics of complexes **C1**−**C3** and free alizarin were evaluated in dimethyl sulfoxide (DMSO) solvent. Free alizarin displays an intense fluorescence emission (λ_{ex}) at approximately 650 nm, resulting in absorption at 420 nm ($\pi \rightarrow \pi^*$), as previously described in the literature.[42] In the spectra of the complexes, only **C1** showed fluorescence when excited at λ_{ex} 414 nm (maximum intensity found for $\pi \rightarrow \pi^*$ present in the spectra of the complexes), resulting in a broad band emission, such as that observed for alizarin, in the region of 550−800 nm (Figure 2). This effect is a consequence of the phosphine ligands in the

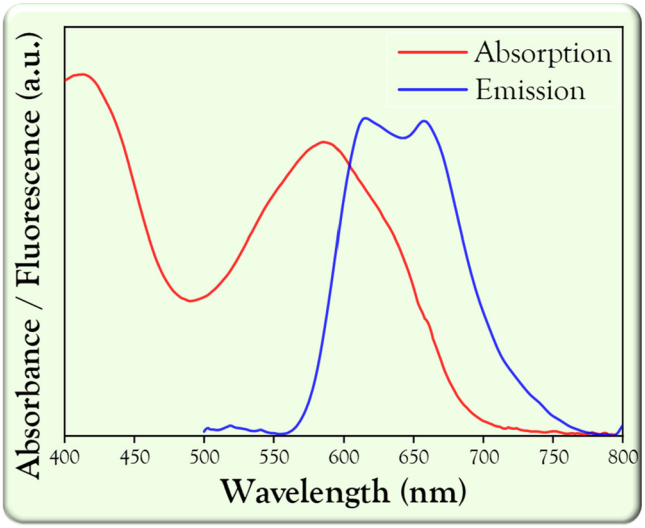

Figure 2. Normalized emission and absorption spectra of **C1** in DMSO (λ_{ex} = 420 nm, 100 μM).

coordination sphere of the complexes, which promote suppression of the fluorescent emission processes when associated in the same complex (fluorescent dye and phosphine).[43,44] Quantum yield calculations confirmed the same trend as the observed in the recorded spectra, using 5,10,15,20-tetra(4-pyridyl)porphyrin (TPyP) as a standard (DMSO, 100 μM), where complex **C1** showed a quantum yield 20 times higher than those of the other complexes and similar to that of free alizarin, as seen in Table 1.

The crystal structures of complexes **C1** (Figure 3A) and **C3** (Figure 3D) were determined by single-crystal X-ray diffraction. Both complexes crystallized in the monoclinic $P2_1/c$ space group, presenting one molecule per asymmetric unit and the PF_6^- counterion in the **C3** structure. The **C3** asymmetric unit showed positional disorders in the *p*-cymene ligand (refined in two positions with 50% occupancy), triethylphosphine (refined in two positions with occupancies of 45% and 55%), and the PF_6^- counterion (refined in two positions with 50% occupancy). The structure confirms the six-membered ring resulting from the coordination of alizarin to ruthenium besides η^6-coordinated *p*-cymene. The $O_1-Ru_1-O_3$, $O_1-Ru_1-Cl_1$, and $O_3-Ru_1-Cl_1$ bond angles of **C1** were 85.8(1), 84.1(2), and 84.8(2)°, respectively, and the $O_1-Ru_1-O_3$, $O_1-Ru_1-P_1$, and $O_3-Ru_1-P_1$ bond angles of **C3** were 85.3(2), 88.3(2), and 85.0(2)°, respectively. The principal bond lengths of the complexes are shown in Table 2. The main change in the alizarin bond lengths is observed for C_3-O_3, which after coordination acquires greater double-bond character, as was also observed in the ^{13}C NMR experiments.

To better understand the crystal structure and rationalize possible intermolecular interactions, we calculated the full interaction maps around the complex molecules using the *Mercury* program.[45,46] Parts B and E of Figure 3 show the interaction maps for **C1** and **C3**, respectively. The blue regions highlight the hydrophilic region (uncharged NH nitrogen probe), the red regions indicate the hydrophobic positions (carbonyl oxygen probe), and the green regions indicate likely positions of aromatic interactions (aromatic CH carbon probe). The profiles obtained for the maps in both molecules were similar, showing the same regions with a probability of intermolecular interactions. The regions in blue stand out, mainly around the uncoordinated O atoms, where there is a great chance of acting as a hydrogen acceptor, while the red regions dominate in the vicinity of the H atoms. The main difference between these maps is the red region around the OH group of **C1**, which is blocked in **C3** due to steric hindrance caused by phosphine. The most abundant intermolecular contacts are of the H···H type, corresponding to practically half of the existing contacts (Figure 3F).

In the fingerprint 2D plots of **C1** (Figure 3C) and **C3** (Figure S18), the H···H contacts for **C3** are approximately 0.8 Å (di/de), while in **C1**, they are approximately 1.1 Å (di/de), showing that the hydrophobic interactions involving **C3** molecules are shorter and more intense, contributing to the formation of aggregates in solution and consequently cooperating with the suppression of fluorescence observed for **C3**. These abundant hydrophobic interactions are also characteristic of substances with predominant lipophilic character and are important in interactions with biomolecules.

The stability of the complexes in solutions, such as those used in the biological tests, was evaluated using the ^1H NMR technique in DMSO-d_6. Thus, the spectrum of complex **C1** exhibits three specific regions, which can be seen by following the signal referring to the propyl group from *p*-cymene (Figure S19 of SI), which presents three independent groups of signals. This may be the result of labilization of the chlorido ligand, which in the presence of other coordinating molecules (DMSO or water) can be replaced by them. This process is widely discussed in the literature because this fact allows coordination of the metal to biomolecules, such as DNA or proteins.[47,48] Complexes **C2** and **C3** were also evaluated in terms of their stability in the cell culture medium (RPMI) and DMSO (2:1) and pure DMSO, adopting the $^{31}P\{^1H\}$ NMR technique. Both complexes were stable in pure DMSO (48 h of experiment), and in the DMSO/RPMI mixture, at the beginning of the experiment, the formation of two additional signals at δ 24 and 28 ppm for **C2** and at δ 22 and 25 ppm for **C3** wwa observed, which remained as the minority species up to 48 h (approximately 20%). The original complexes remained as the majority species, as shown in Figure S20. The signals at δ 24 ppm for **C2** and δ 22 ppm for **C3** can be related to the precursors **P2** and **P3**, respectively, which have the same chemical shifts. The appearance of signals referring to precursors **P2** and **P3** can be favored by two factors: The first is due to labilization of a O,O-coordinated ligand, as was

https://doi.org/10.1021/acs.inorgchem.3c00183
Inorg. Chem. 2023, 62, 6955−6969

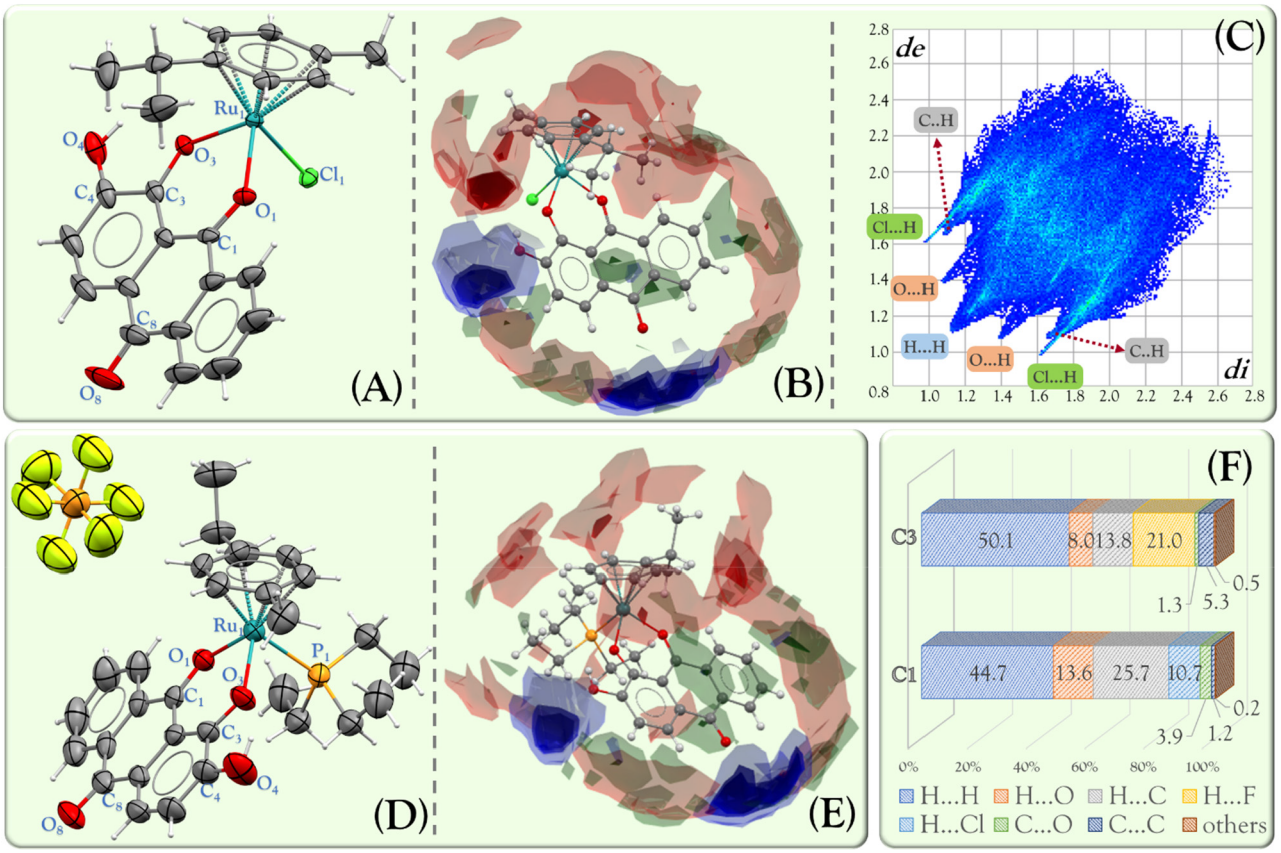

Figure 3. (A) Crystal structure of **C1** (30% of thermal ellipsoids). (B) Interaction map for complex **C1**. (C) Full fingerprint 2D plot for complex **C1**. (D) Crystal structure of **C3** (30% of thermal ellipsoids). (E) Interaction map for complex **C3**. (F) Percentage of each contact type for complexes **C1** and **C3**.

Table 2. Selected Bond Lengths of C1, C3, and the Alizarin Crystal Structure

	C1	C3	alizarin[a]
Ru_1-O_1	2.075(3)	2.068(6)	
Ru_1-O_3	2.057(2)	2.063(5)	
Ru_1-P_1		2.350(2)	
Ru_1-Cl_1	2.439(1)		
Ru_1-cp[b]	1.652	1.694	
C_1-O_1	1.252(5)	1.25(1)	1.245(7)
C_3-O_3	1.295(5)	1.29(1)	1.347(5)
C_4-O_4	1.339(7)	1.35(1)	1.343(5)
C_8-O_8	1.239(7)	1.21(1)	1.224(7)

[a]CCDC 800614. [b]cp = centroid of *p*-cymene.

already reported for ruthenium/arene complexes.[49] The second is due to the fact that the culture medium used in this experiment has a high free chloride content, which also favors the formation of precursors in solution. However, in the present study and under the conditions tested for **C2** and **C3**, this speciation occurred only on a small scale, with **C2** and **C3** remaining as the majority species in solution.

DNA Interaction Experiments. Knowing the strength and type of binding of metal complexes with DNA is relevant information for investigating possible mechanisms of action against tumor cells. The cytotoxic activity of cisplatin is partly attributed to its ability to bind to DNA, interfering in the mechanisms of repair of DNA and triggering cell death pathways.[50,51]

Based on UV−vis absorption spectroscopy, the $\pi \rightarrow \pi^*$ transition bands exhibited by the complexes were monitored to observe a possible decrease in intensity (hypochromism) or displacement (bathochromism) of these bands with successive additions of calf thymus DNA (*ct*-DNA) solutions. The affinity between the complex and DNA can be measured by calculating the binding constant (k_b, from neighbor-exclusion equation), which is dependent on the maximum absorption of the transition bands present in the spectrum. As can be seen in Figure 4, when DNA aliquots are added to a solution containing the complexes, a decrease in the absorption intensity (hypochromic effect) of the bands is observed. This effect is due to dilution of the solution and to variations in the complex electronic transition energies, causing changes in the absorption intensity due to interactions between the complex and DNA. To evaluate the contribution of the dilution effect for each complex, an experiment was carried out separately by adding aliquots of buffer, determining the hypochromism that resulted from complex dilution. The hypochromism values (discounting the dilution effect) resulting from this experiment show that practically only complex **C1** interacts with DNA, presenting 25% hypochromism, while **C2** and **C3** present irrelevant hypochromism values. Complex **C1** displays a k_b constant value equal to $2.5 \times 10^4 \pm 0.6 \times 10^4$, with a magnitude of 10^4 corresponding from a medium/strong interaction with DNA.[52−55]

Because complexes such as **C1**, with a labile chlorido ligand, establish their anticancer effects by coordinating to the *N*7-guanine units in DNA, the moderate/strong interaction

https://doi.org/10.1021/acs.inorgchem.3c00183
Inorg. Chem. 2023, 62, 6955−6969

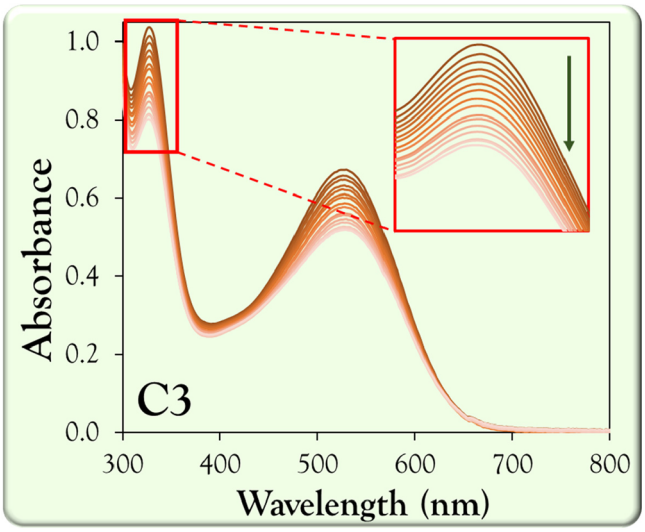

Figure 4. Absorption spectra in the UV−vis region obtained for complex **C1** with the addition of successive aliquots of *ct*-DNA.

observed for **C1** may be a result of the existence of covalent complex/DNA interaction. To confirm this observation, we performed assays with plasmid DNA (PBR322), using the gel electrophoresis technique, adopting solutions with [complex]/[DNA] molar ratios of 0.25, 0.5, 1.0 and 1.5, in which all of the samples were preincubated, under stirring for 24 h, at 37 °C. Figure S21 presents the results obtained for these experiments. Comparing the bands displayed in the experiments containing the complexes with those of the negative control (DNA + DMSO), we observed that the **C2** and **C3** compounds did not induce changes in the position and intensity of the supercoiled DNA bands, showing that there are no interactions between the complexes and DNA, as seen in the spectrophotometric titration experiments. Complex **C1** exhibited a different result, showing complete disappearance of the bands at higher concentrations, which is characteristic of a strong interaction between the complex and DNA, as we observed for the positive control (cisplatin). Thus, on the basis of the results of the spectroscopic titrations and electrophoresis, we suggest that the existence of interactions of the covalent type for complex **C1** may be predominant in relation to other types of interaction, which is able to compose its mechanism of action against cancer cells, similar to other ruthenium/arene/chlorine complexes described in the literature.[56,57]

Biological *In Vitro* Experiments. The cytotoxic profile of the complexes was evaluated in human tumor cell lines MDA-MB-231 (breast cancer), MCF-7 (breast cancer), and A549 (lung cancer) and nontumor cell lines MCF-10A (breast) and MRC-5 (lung). The tests were carried out using cell treatment protocols and using DMSO as a solvent but without exceeding the limit of 0.5% of the final volume, in which the period of exposure of cells to the complexes is equal to 48 h. The IC_{50} values (concentration of the complex capable of inhibiting 50% cell proliferation) found for the complexes, alizarin, and precursors against the different cell lines cited above are shown in Table 3.

Precursors **P1** and **P3** and alizarin (L) did not present cytotoxicity toward the cells at the highest concentration tested (100 μM), while precursor **P2** showed considerable cytotoxicity, even with values close to those shown by cisplatin in nontumor cells. Complex **C2** exhibited greater inhibition of cytotoxicity against the cells, presenting in all cases IC_{50} values at least 3 times lower than those of **C1** and **C3** and slightly lower than that of cisplatin in MDA-MB-231 and MCF-10A cells. When complexes and precursors are compared, it can be observed that in all cases the compounds containing triphenylphosphine as the ligand are the most active (**C2** and **P2**), showing considerably lower values than the others, in all cell lines tested. This fact may be correlated with the higher lipophilicity exhibited by triphenylphosphine complexes, giving complex **C2** a high value of partition coefficient *n*-octanol/water (log P = 0.61 ± 0.02), while in the complex with triethylphosphine (**C3**), this value is equal to 0.30 ± 0.04; therefore, PPh_3 confers additional lipophilicity to the complex than the corresponding PEt_3-containing complex, which, in turn, was more lipophilic than complex **C1**, which lacks monophosphine and exhibits a lower log P value (0.17 ± 0.08).[59,60]

It is known that lipophilic compounds have greater affinity with the membrane proteins of eukaryotic cells, where through interactions with these proteins (including the hydrophobic interactions cited in the crystallographic discussion), these molecules become more likely to undergo active transport from the extracellular to intracellular environment and are able to trigger mechanisms of cell death in the interior of cells. Thus, the lower IC_{50} value displayed by the **C2** compound may be correlated with this characteristic. This compound is more lipophilic, which can lead to a greater ability to accumulate inside the cells and inhibit the proliferative ability, and this fact, to be confirmed, requires the performance of other cell permeation experiments. Table 3 also shows the selectivity values found for the complexes, where only in the breast cells was there selectivity for tumor lineages, ranging from 0.9 to 1.7. However, the selectivity exhibited by the complexes is

Table 3. IC_{50} Values (μM) and Selectivity Indexes[a] Obtained for C1−C3, Alizarin (L), Precursors P1−P3, and Cisplatin (CP) against Tumor and Nontumor Cell Lines in the Period of 48 h

	MDA-MB-231	MCF-7	MCF-10A	A549	MRC-5	IS_1	IS_2	IS_3
C1	42.2 ± 3.6	32.8 ± 1.2	57.0 ± 0.6	>100	53.9 ± 0.5	1.3	1.7	
C2	6.5 ± 0.1	9.0 ± 0.1	10.0 ± 0.3	17.8 ± 0.8	7.7 ± 0.1	1.5	1.1	0.4
C3	45.4 ± 1.4	>100	41.6 ± 0.1	52.6 ± 1.2	25.0 ± 0.1	0.9		0.5
L	>100	>100	>100	>100	>100			
P1	>100	>100	>100	>100	>100			
P2	46.8 ± 0.6	>100	18.2 ± 0.6	41.2 ± 0.3	23.9 ± 0.1	0.4		0.6
P3	>100	>100	>100	>100	>100			
CP[58]	10.2 ± 0.2	8.6 ± 1.8	14.0 ± 2.0	14.4 ± 1.4	29.1 ± 0.8	1.4	1.6	2.0

[a] IS_1 = IC_{50}(MCF-10A)/IC_{50}(MDA-MB-231); IS_2 = IC_{50}(MCF-10A)/IC_{50}(MCF-7); IS_3 = IC_{50}(MRC-5)/IC_{50}(A549).

https://doi.org/10.1021/acs.inorgchem.3c00183
Inorg. Chem. 2023, 62, 6955−6969

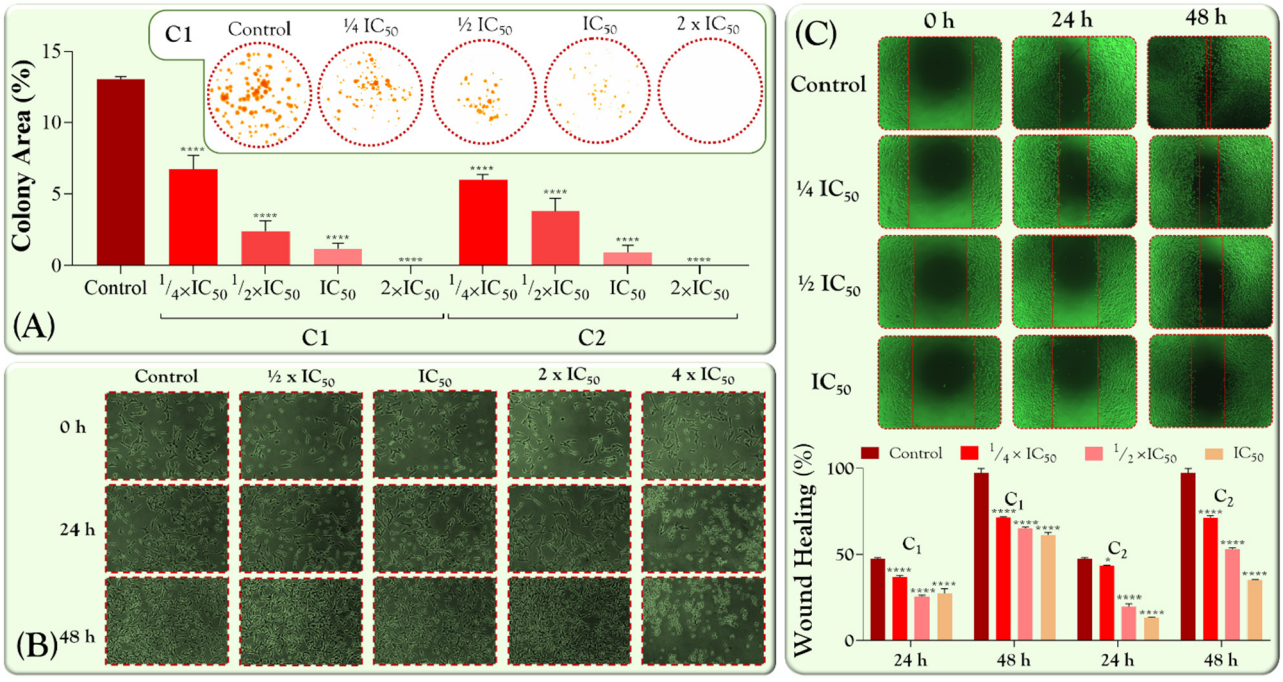

Figure 5. (A) Micrographs of clonogenic assay showing MDA-MB-231 cells treated with complex **C1** and graphs of quantifications of the colony area. (B) Effects of complex **C2** on the cell morphology of MDA-MB-231, after exposure of 0, 24, and 48 h. (C) Effect of complex **C1** on MDA-MB-231 cell migration by using an inverted microscope (4×) and graph of the wound-healing closure percentages for treatment with **C1** and **C2**. These experiments were representative of three independent assays. Significance at (****) $p < 0.0001$ using ANOVA. Solvent control experiments were performed with DMSO (1%).

lower than that found for cisplatin because they had a strong cytotoxic effect on nontumor cell lines.

Aiming to explore the influence of the substances on the morphology of MDA-MB-231 cells, we selected complexes **C1** and **C2** to be evaluated because they were the ones that presented the highest selectivity indexes among the complexes described in this work. The cells were treated with concentrations of complexes proportional to the IC_{50} values ($^1/_2 \times IC_{50}$, IC_{50}, $2 \times IC_{50}$, and $4 \times IC_{50}$), and the images were recorded at times of 0, 24, and 48 h. In addition, a similar experiment was performed with solvent control (1% DMSO). Analyzing the resulting images (Figure 5B), we observed that **C2** did not cause significant changes in concentrations equal to $^1/_2 \times IC_{50}$, IC_{50}, and $2 \times IC_{50}$, demonstrating that under these conditions the cells maintain their morphological integrity and are indistinguishable from the control experiment. The most significant change is observed only at the concentration equal to $4 \times IC_{50}$, where already in 24 h of experiment the cells show changes in their morphology and a loss of adhesion to the bottom of the plate. Besides these observations, complex **C1** in 48 h at a concentration of $2 \times IC_{50}$ displays a loss of cell confluence (Figure S22).

To evaluate the cytostatic effect of the complexes on the MDA-MB-231 cell line, we performed clonogenic survival assays, where it is possible to determine the ability of a cell to proliferate, forming a colony of cells (important step in the metastatic process), after being exposed to different concentrations of the complexes ($^1/_4 \times IC_{50}$, $^1/_2 \times IC_{50}$, IC_{50}, and $2 \times IC_{50}$) for 48 h. After this period, the culture medium containing the complexes was discarded and a new medium was added, and the surviving cells were incubated again, for 10 days, for growth of the resulting colonies.[61,62] Both complexes (**C1** and **C2**) display antiproliferative activity, inducing the cells to lose their clonogenicity with an increase of the concentration of the complexes, where in a concentration of $2 \times IC_{50}$, complete inhibition of the ability of cells to form colonies (Figure 5A) was observed. This result is interesting because, even maintaining the morphology of the cells (as observed in the morphological assay), at the concentration of $2 \times IC_{50}$, the cells appear to suffer irreversible damage, directly affecting their ability to form colonies, suggesting a possible antimetastatic action of the **C1** and **C2** compounds. The concentration-dependent effect can be seen in Figure 5A, which shows the resulting colony area as a function of the total area of the well, where the decrease in the colony area with increasing concentration is considerable and significant.

Another important information that contributes to the antimetastatic activity of the complexes is their ability to inhibit the migration of cells, which in this work was done following the collective migration of cells in an empty strip made in a monolayer of the cells. To do this, we used MDA-MB-231 cells treated with complexes at concentrations equal to $^1/_4 IC_{50}$, $^1/_2 IC_{50}$, and IC_{50}, recording the images at 0, 24, and 48 h of experiment. When the results displayed in Figure 5C are analyzed, it can be concluded that the negative control experiment (1% DMSO), in 48 h, practically closed the empty space, while at concentrations equal to $^1/_2 IC_{50}$ and IC_{50}, a similar pattern was not observed. This observation becomes clearer upon analysis of the percentage of the closure presented in the graph of Figure 5C, where in the control, the empty area decreases by 50% (24 h), while in the **C1** complex (IC_{50} concentration), this decrease is 24%, and with **C2**, it is even lower, closing at just 13%. In 48 h, the control displays the wound healing practically completed; however, in all treatments, migration inhibition was observed, where the **C2** compound exhibited the highest inhibition. It is important to

https://doi.org/10.1021/acs.inorgchem.3c00183
Inorg. Chem. 2023, 62, 6955−6969

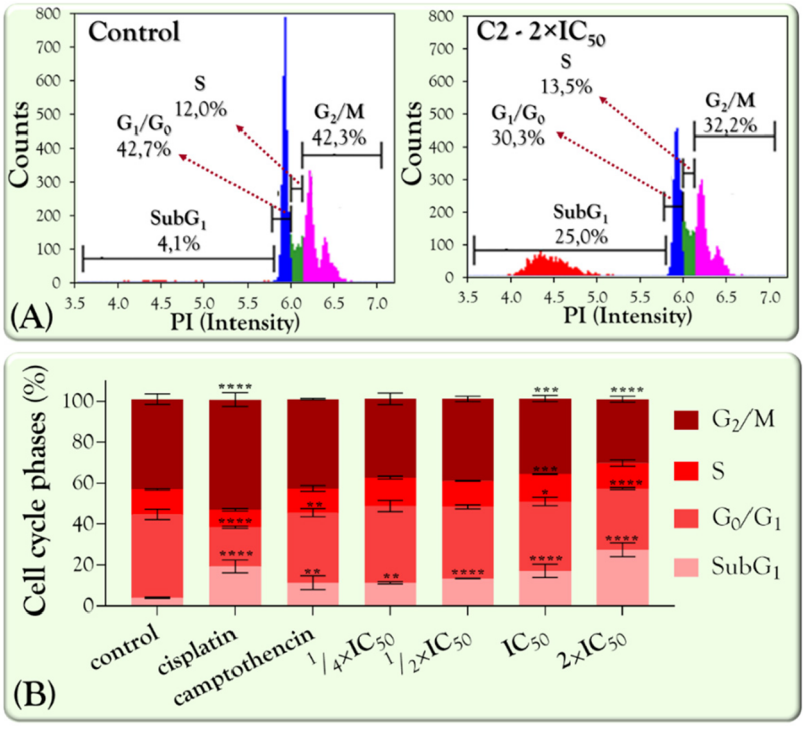

Figure 6. (A) Cell count distribution for phases G_2/M, S, G_1/G_0, and Sub-G_1 of the negative control and complex **C2**. (B) Percentage of cells in each phase of the cell cycle at different concentrations of complex **C2**: (*) $p < 0.05$; (**) $p < 0.01$; (***) $p < 0.001$; (****) $p < 0.0001$. Solvent control experiments were performed with DMSO (1%).

point out that the migration inhibition effect was also observed at concentrations lower than the IC_{50} concentration, which indicates that the observed effect is mainly due to the inhibition of cell migration and not to the cytotoxic effect of the tested compound. These results place the compounds among an important class of substances that have antimetastatic activity, such as NAMI-A and the ruthenium(II)/arene analogue RAPTA-C, which exhibit *in vivo* and *in vitro* antimetastatic activity, in addition to having already been evaluated in advanced clinical trials.[63−65]

Knowing that the complexes have antiproliferative and probable antimetastatic activity against MDA-MB-231 cells, analysis of the effect of complex **C2** ($^1/_4IC_{50}$, $^1/_2IC_{50}$, IC_{50}, and $2 \times IC_{50}$) on the cell cycle distribution was performed. Figure 6A shows the distribution of cells in the phases of the cell cycle for the control experiments and in the concentration of $2 \times IC_{50}$ of complex **C2**. When these graphs are compared, it can be observed that complex **C2** triggers changes in the cell cycle of MDB-MB-231 cells, leading to an increase in the number of cells in the Sub-G_1 phase and a decrease in the G_2/M and G_1/G_0 phases. In Figure 6B, these trends become clearer when a significant increase in the number of cells in the Sub-G_1 phase with an increase in the concentration of the complexes is visualized. The decrease in the number of cells in G_2/M is an indication that the damage caused to cellular structures is difficult to repair, leading to a consequent increase in cells in Sub-G_1, which is a natural cell response to the damage caused, leading to the activation of cell death mechanisms by apoptosis.[66−70]

Although there are mechanisms of cell death that can be triggered through interactions with membrane proteins or with components of the extracellular matrix, there are several other known mechanisms that occur involving molecules present in the nucleus and cytoplasm of the cells. Thus, upon exploration of the fluorescence of complex **C1**, the treatment of MDA-MB-231 cells using the concentration of IC_{50} (40 μM) was performed to visualize the complex uptake by the cells.

As shown in Figure 7A, the flow cytometry obtained for cells MDA-MB-231 treated with complex **C1** showed that this complex does not accumulate in viable cells, either at 24 h or at 48 h, without altering the fluorescence profile displayed by the cells. Free alizarin is also not internalized by the cell, as shown in Figure 7B. When a fluorescent compound is internalized by the cells, the distribution of fluorescence displayed by the cells is altered as the fluorophore accumulates, unlike that observed for alizarin and complex **C1**. Using confocal microscopy, we sought to confirm what was observed in the previous experiment. To delimit the nucleus of the cells, we used the DNA marker DAPI, which when irradiated at 360 nm, exhibited fluorescence at 460 nm, showing blue staining. To capture the fluorescence from complex **C1**, the cells were irradiated at 420 nm (maximum absorption of the band responsible for fluorescence). As shown in Figure 7E, at first, internalization of the complex by the cells was not observed, showing only the fluorescence inherent to the cell nucleus marker (DAPI). Internalization of the complex was only observed after permeabilization of the cells (Figure 7F), exhibiting fluorescence in the red spectral region (650 nm), as is seen in the quantum yield calculation experiments. This information shows that this complex is internalized in the cells only after the damage done to the cell membranes, not being able to be internalized by viable cells. These data provide important information, showing us that the complex is unable to be internalized by the cell probably due to the low lipophilicity exhibited by this complex compared with the others with phosphines. Consequently, because the **C1**

https://doi.org/10.1021/acs.inorgchem.3c00183
Inorg. Chem. 2023, 62, 6955−6969

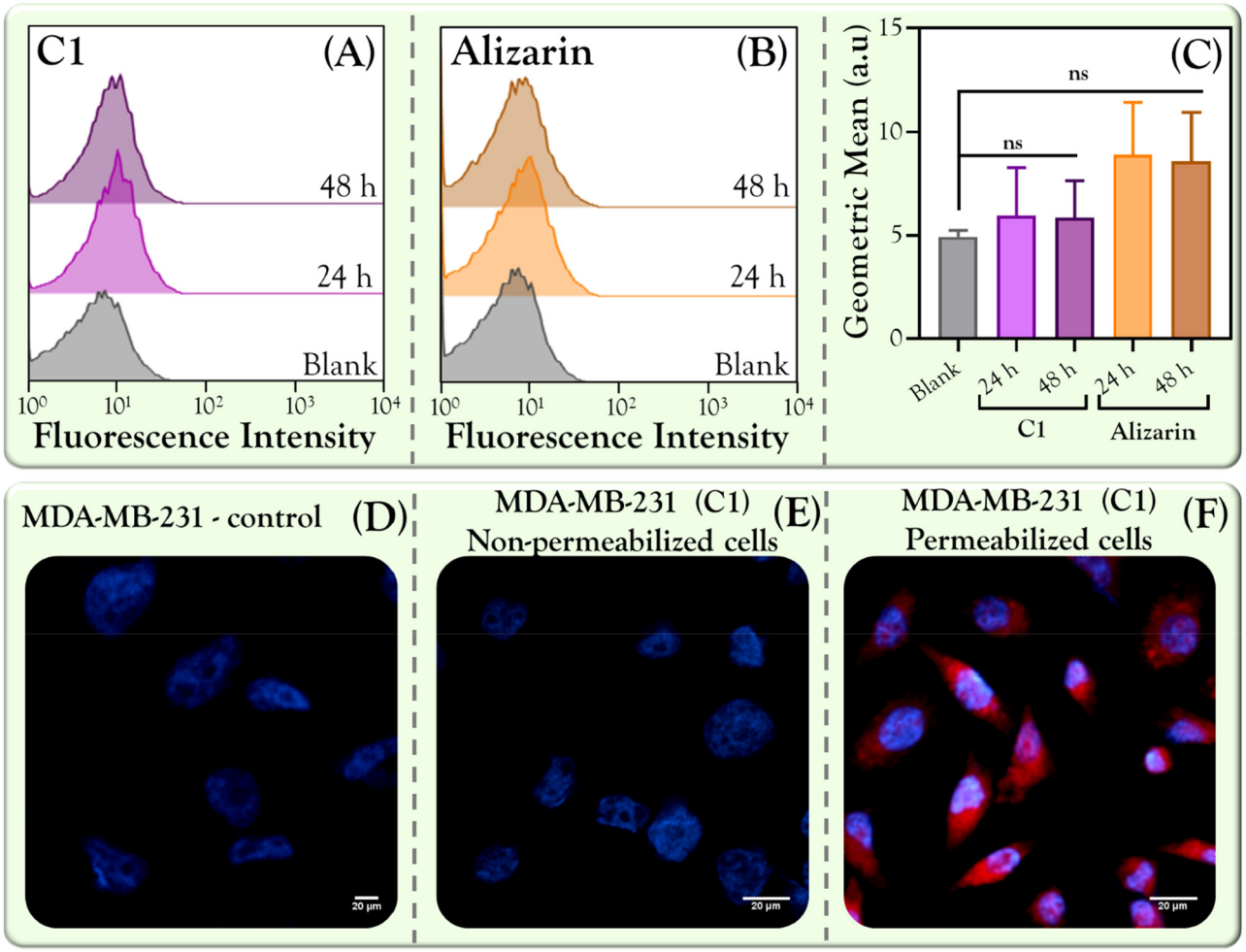

Figure 7. Flow cytometric analysis of MDA-MB-231 cells incubated with (A) a blank solution and **C1** for 24 and 48 h and (B) a blank solution and alizarin for 24 and 48 h. (C) Quantification of the mean fluorescence intensity (geometric mean) of the histograms. Data represent mean ± SD of the assays in triplicate. Significance at the levels (ns) was determined using one-way ANOVA and Dunnet's test. Fluorescent imaging of (D) MDA-MB-231 cells incubated with a blank solution (negative control), (E) nonpermeabilized MDA-MB-231 cells incubated with **C1**, and (F) MDA-MB-231 cells permeabilized with 01% Triton-X 100 in PBS and incubated with **C1**. The nuclei were stained with Hoechst 33342 (blue channel). All images were acquired for both channels (blue and red).

complex is not internalized, the interactions with molecules in the intracellular environment do not occur, thus triggering internal cell death mechanisms, maintaining the normal functioning of the cell and justifying the high IC_{50} value found.

Biological *In Vivo* Experiments. In this study, an early toxicological screening of new ruthenium-based anticancer drugs using the zebrafish model was performed as a strategy to avoid late-stage failures of the development of new drugs and reduce cost and time. Differential mortality rates were observed in the zebrafish embryo–larval stages after exposure to the **C1**–**C3** compounds and free alizarin, which were compared to negative and solvent groups (Figures S23A–D). As expected, zebrafish embryos exposed to negative control and solvent control (0.5% DMSO) groups did not present mortality, which demonstrates a valid test. On the other hand, exposure of animals to ruthenium complexes showed that animal mortality is concentration-dependent. Thus, exposing the zebrafish embryos to complex **C1** caused the highest mortality among the complexes tested, within the first 24 h. At all concentrations tested for complex **C1**, mortality rates between 76 ± 11 and 100 ± 0.0% ($p < 0.001$) were observed (Figure S23A). On the other hand, 7 ± 5% of embryos died at the end of 96 h in the group exposed to 7.5 μM **C2**. Zebrafish embryos exposed to the highest concentrations of **C2** (15 and 30 μM) presented mortality rates of 60 ± 0% and 93 ± 11% at 96 h ($p < 0.001$), respectively (Figure S23B). Similarly, exposure of animals to complex **C3** at low concentration did not lead to embryo mortality; however, at high concentrations of **C3** (30 and 60 μM), the mortality rates were 66 ± 15% and 93 ± 11%, respectively (96 h) (Figure S23C). Exposure of the animals to free alizarin at both concentrations (15 and 30 μM) caused 33 ± 15% and 83 ± 11%, respectively, of embryonic mortality ($p < 0.001$) at 96 h (Figure S23D).

The hatching rate was also evaluated in zebrafish after exposure to complexes **C1**–**C3** and free alizarin (Figures S23E–H). Exposure of the zebrafish embryos to the complexes inhibited hatching, while the embryos from the control groups hatched normally. At all concentrations tested, exposure of the animals to complexes **C1** and **C3** and free alizarin caused hatching inhibition in zebrafish. On the other hand, exposure of the animals to complex **C2** at the lowest concentration caused hatching delays. Thus, while 100% zebrafish hatched until 96 h, for the group exposed to 7.5 μM **C2**, 76 ± 15% hatched embryos at 96 h ($p < 0.05$) was observed. However,

https://doi.org/10.1021/acs.inorgchem.3c00183
Inorg. Chem. 2023, 62, 6955–6969

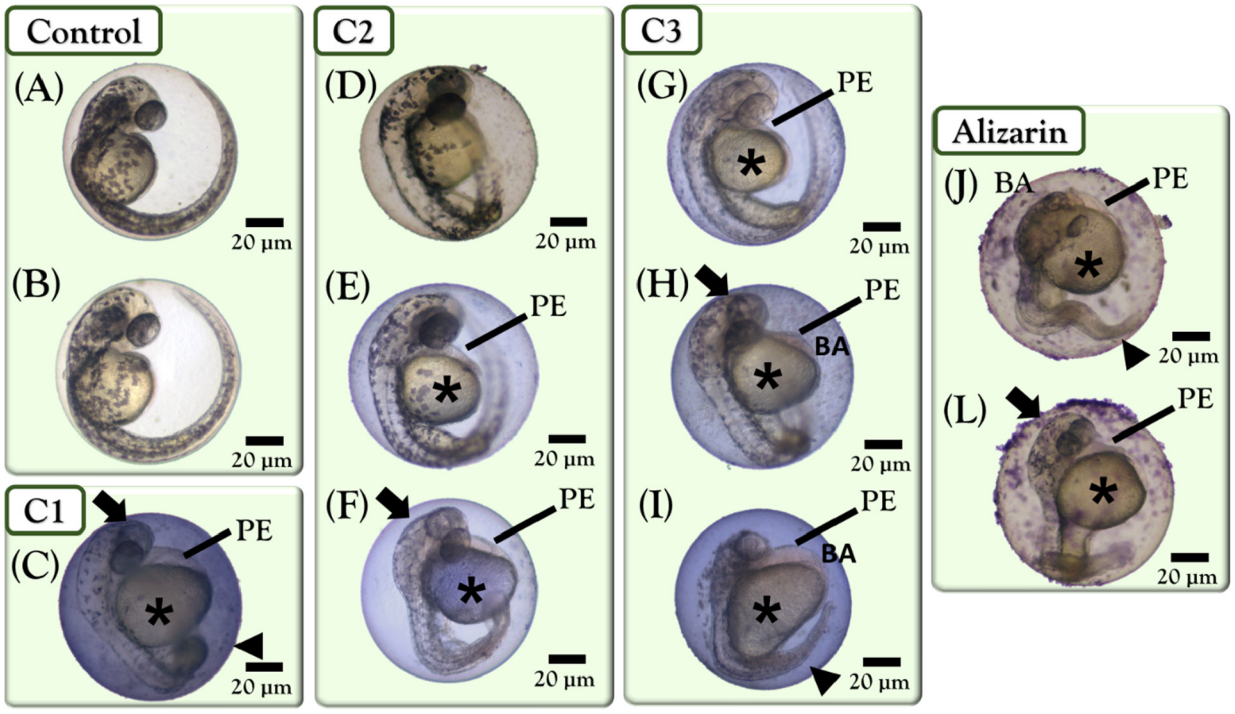

Figure 8. Morphological changes in the zebrafish embryos after 48 h of exposure to **C1**−**C3** and L: (A) negative control group (without treatment or solvent); (B) solvent control group; (C) **C1** at 15 μM; (D) **C2** at 7.5 μM; (E) **C2** at 15 μM; (F) **C2** at 30 μM; (G) **C3** at 15 μM; (H) **C3** at 30 μM; (I) **C3** at 60 μM; (J) alizarin at 15 μM and alizarin (L) at 30 μM. Arrow = head changes; arrowhead = tail changes; asterisk (*) = yolk sac changes; BA = blood accumulation; PE = pericardial edema.

the other concentrations of complex **C2** tested also caused hatching inhibition in zebrafish.

Besides mortality, both **C1** and **C3** caused a higher hatching failure of zebrafish embryos. Interestingly, the hatching failure was a common end point reported in other toxicological screening of ruthenium complexes.[71−77] In this model, toxicity evaluation considers hatching success to be a sensitive end point. Hatching of all embryos until 96 h is expected; however, when hatching failure occurs, it means that the compounds under testing can interfere with the normal biological development of zebrafish. Moreover, embryos that did not hatch evolve to death.[78]

Morphological changes were recorded in zebrafish upon exposure to the ruthenium complexes (Figure 8). Exposure to both compounds, **C2** and **C3**, induced several malformation phenotypes in zebrafish embryos, such as head malformation, somite malformation, tail malformation, delayed growth, pericardial edema, yolk sac edema, and interaction with chorion (Table S2). The exposure at 15 μM **C1** caused edema in the pericardium and yolk sac of 17 ± 6% zebrafish alive ($p < 0.05$) and 20% of them interacted with chorion ($p < 0.05$). For the group exposed to **C2** at the lowest concentration, there were no significant alterations in the development of the zebrafish embryos. However, delayed growth, pericardial edema, yolk sac edema, and interaction with chorion were observed in zebrafish exposed to **C2** at high concentrations (15 and 30 μM; $p < 0.001$). On the other hand, all **C3** concentrations induced morphological changes in live zebrafish, such as chorion alteration (15−60 μM; $p < 0.001$), pericardial edema (15 and 30 μM; $p < 0.001$), yolk sac edema (30 μM; $p < 0.001$), and growth retardation (60 μM; $p < 0.001$). Interaction with chorion includes changing its color, which probably suggests the accumulation of these metal complexes in zebrafish chorion (Figure 8C,E−L). Besides edema in the pericardium and yolk sac and delayed growth, exposure to alizarin caused head, somite, and tail malformation in zebrafish alive at 15 μM.

Yolk sac edema has been considered to be a sensitive toxicological response for embryo toxicity. It is noteworthy that the yolk sac is metabolically active and highly lipophilic. However, exposure to chemical substances can decrease yolk utilization/mobilization, resulting in impaired embryonic nutrition that affect its entire development.[79] Moreover, osmoregulation of the zebrafish embryos can also be altered, resulting in excessive uptake of the substance to which it was exposed. As a consequence, edema is formed, and the substance may accumulate in the embryo.[80] Gills, the digestive system, and kidney are responsible for osmoregulation of zebrafish.[81] Until these structures become functionally active, osmatic balance is maintained for two water permeability barriers on the surface of the embryo and one surrounding the yolk sac.[80] Therefore, the tested compounds may impair the embryonic nutrition and/or maintenance of the permeability barrier, causing edema in the yolk sac and pericardium and bioaccumulation.

Anticancer agents present clinical concerns with their systemic toxicity. Among the side effects, neurotoxicity, vascular toxicity, nephrotoxicity, and ototoxicity are the most common.[82] Therefore, overcoming the unpleasant side effects is a major challenge concerning new anticancer agents.

Besides the classic biomarker (mortality, hatching rate, and morphological change), multiple biomarker responses can be explored using a zebrafish model system in early preclinical toxicological screening, including neurotoxicity and cardiotoxicity. The neurotoxic effect of ruthenium/alizarin complexes was determined in zebrafish embryos at 24 h by analyzing the

https://doi.org/10.1021/acs.inorgchem.3c00183
Inorg. Chem. 2023, 62, 6955−6969

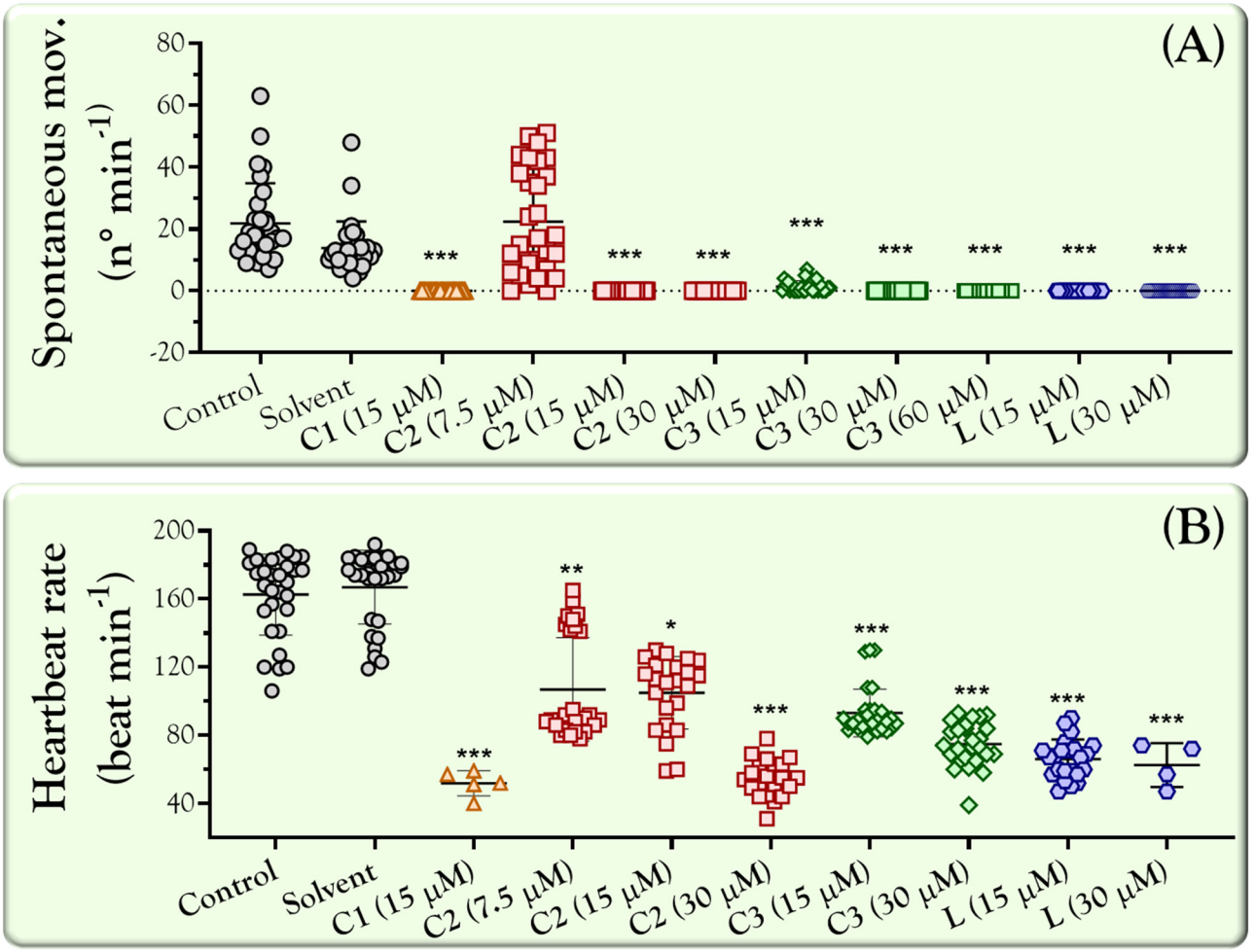

Figure 9. (A) SCF (no. min^{-1}) and (B) heartbeat rate (beats min^{-1}) of zebrafish embryos alive from negative control and solvent groups and after exposure to **C1**−**C3** and alizarin for 24 h (SCF) and 48 h (heartbeat rate). Dots touching the *x* axis at 0 indicate embryos alive but lacking movement during the analysis. (*) $p < 0.05$ versus negative control, (**) $p < 0.01$ versus negative control, and (***) $p < 0.001$ versus negative control.

frequency of spontaneous movements (SCF). As shown in Figure 9A, only exposure of the zebrafish embryos to **C2** at low concentration did not cause neurotoxicity. The SCF is an important parameter of neurotoxicity because spontaneous tail coiling is the first motor activity as a consequence of innervation of the muscle by the developing nervous network,[82] which could reflect a morphological effect or even mortality.[82] Therefore, hatching failure and morphological change, including delayed growth, somite, and tail malformation, in embryos and mortality can be related to the neurotoxic effect of the compounds.

The cardiotoxicity, one of the most common side effects of anticancer agents,[82] was analyzed in the zebrafish embryos at 48 h after exposure to the compounds (Figure 9B). As expected, a normal embryonic heart rate was recorded for the control (without complexes and solvent) and solvent groups, at 162 ± 24 and 167 ± 21 beats min^{-1}, respectively. In contrast, all exposure of the zebrafish embryos to the ruthenium complexes causes alterations in the heartbeat rate of zebrafish compared to embryos from control groups. Zebrafish embryos exposed to **C1** and **C3** and free alizarin showed the lowest heart rates, from 52 to 93 beats min^{-1}. A decrease in the heartbeats, at 106 ± 30 and 105 ± 21 beats min^{-1}, was observed in zebrafish exposed to **C2** (7.5 and 15 μM, respectively) compared to the control group ($p < 0.05$).

The heartbeat frequency can be obtained at 48 hpf because major heart structures have been formed in zebrafish. However, because its heart is still immature, cardiac function can influence the development of the whole animal.[83] Furthermore, a decrease of the heartbeat in the early embryonic development of zebrafish can lead to animal death.[78] In this study, the cardiotoxicity classified as bradycardia may be associated with the mortality rate and morphological change because pericardial effusion can cause blood congestion, decreasing blood flow and consequently decreasing the heartbeats. In fact, pericardial edema consisted of the main morphological alterations observed. It is important to note that embryos exposed to 7.5 μM **C2** did not present significant morphological change.

Taken together, **C1** and **C3** showed greater toxicity to the development of the zebrafish embryo. On the other hand, **C2**, the most promising anticancer drug in *in vitro* preclinical tests, revealed the lowest toxicity in *in vivo* preclinical screening using zebrafish as a model system.

https://doi.org/10.1021/acs.inorgchem.3c00183
Inorg. Chem. 2023, 62, 6955−6969

CONCLUSION

In this work, a new series of three ruthenium/arene/alizarin complexes containing chlorido or monophosphine ligands were synthesized and characterized. Complex **C1** exhibits strong covalent DNA interaction due to the presence of the labile chlorido ligand in its structure. Complex **C2** was the most selective and cytotoxic toward breast cancer cells (MDA-MB-231), exhibiting IC_{50} values comparable to those of cisplatin. Fluorescence studies showed that complex **C1** exhibits fluorescence like free alizarin does and it cannot be internalized in MDA-MB-231 cancer cells probably due to its low lipophilicity. Complexes **C1** and **C2** were selected for detailed studies on MDA-MB-231 cells, and it was found that these complexes inhibit colony formation and induce cell cycle arrest in the Sub-G_1 phase in a concentration-dependent manner. Complex **C2** showed quite encouraging outcomes in the *in vitro* setting, as well as *in vivo* toxicological screening at low concentration using the zebrafish model. Therefore, complex **C2** is the most suitable candidate for drug development to treat triple-negative breast cancer.

ASSOCIATED CONTENT

Supporting Information

The Supporting Information is available free of charge at https://pubs.acs.org/doi/10.1021/acs.inorgchem.3c00183.

Measurements, tables, and figures providing the NMR data of the complexes, X-ray crystallographic data, and DNA interaction studies of all complexes (PDF)

Accession Codes

CCDC 2161723 and 2161724 contain the supplementary crystallographic data for this paper. These data can be obtained free of charge via www.ccdc.cam.ac.uk/data_request/cif, or by emailing data_request@ccdc.cam.ac.uk, or by contacting The Cambridge Crystallographic Data Centre, 12 Union Road, Cambridge CB2 1EZ, UK; fax: +44 1223 336033.

AUTHOR INFORMATION

Corresponding Authors

João Honorato de Araujo-Neto − *Instituto de Física de São Carlos, Universidade de São Paulo (USP), São Carlos, São Paulo 13566-590, Brazil; Departamento de Química, Universidade Federal de São Carlos, São Carlos, São Paulo 13565-905, Brazil;* orcid.org/0000-0002-1127-6083; Email: honoratoneto10@gmail.com

Alzir A. Batista − *Departamento de Química, Universidade Federal de São Carlos, São Carlos, São Paulo 13565-905, Brazil*; Email: daab@ufscar.br

Authors

Adriana P. M. Guedes − *Departamento de Química, Universidade Federal de São Carlos, São Carlos, São Paulo 13565-905, Brazil*

Celisnolia M. Leite − *Instituto de Física de São Carlos, Universidade de São Paulo (USP), São Carlos, São Paulo 13566-590, Brazil*

Carlos André F. Moraes − *Departamento de Química, Universidade Federal de São Carlos, São Carlos, São Paulo 13565-905, Brazil*

Andressa L. Santos − *Instituto de Patologia Tropical e Saúde Pública, Universidade Federal de Goiás, Goiânia, Goiás 74605-050, Brazil*

Rafaella da S. Brito − *Instituto de Patologia Tropical e Saúde Pública, Universidade Federal de Goiás, Goiânia, Goiás 74605-050, Brazil*

Thiago L. Rocha − *Instituto de Patologia Tropical e Saúde Pública, Universidade Federal de Goiás, Goiânia, Goiás 74605-050, Brazil*

Francyelli Mello-Andrade − *Instituto de Patologia Tropical e Saúde Pública, Universidade Federal de Goiás, Goiânia, Goiás 74605-050, Brazil; Instituto Federal de Educação Ciência e Tecnologia (IFG), Goiânia, Goiás 74055-110, Brazil;* orcid.org/0000-0001-7389-6125

Javier Ellena − *Instituto de Física de São Carlos, Universidade de São Paulo (USP), São Carlos, São Paulo 13566-590, Brazil;* orcid.org/0000-0002-0676-3098

Complete contact information is available at: https://pubs.acs.org/10.1021/acs.inorgchem.3c00183

Notes

The authors declare no competing financial interest.

ACKNOWLEDGMENTS

We thank the Group of Nanomedicine and Nanotoxicology, Physics Institute of São Carlos (IFSC-USP), for carrying out the flow cytometry and fluorescence experiments. The authors are grateful for financial support provided by CNPq (306329/2020-4), CAPES (finance code 001), and FAPESP (17/15850-0, 21/02522-0, and 21/04876-4).

REFERENCES

(1) World Health Organization. Estimated number of deaths in 2020, all cancers, both sexes, all ages. https://gco.iarc.fr/today/home (accessed Dec 19, 2022).

(2) Lee, S. Y.; Kim, C. Y.; Nam, T.-G. Ruthenium Complexes as Anticancer Agents: A Brief History and Perspectives. *Drug Des. Devel. Ther.* **2020**, *14*, 5375−5392.

(3) Babak, M. V.; Meier, S. M.; Huber, K. V. M.; Reynisson, J.; Legin, A. A.; Jakupec, M. A.; Roller, A.; Stukalov, A.; Gridling, M.; Bennett, K. L.; Colinge, J.; Berger, W.; Dyson, P. J.; Superti-Furga, G.; Keppler, B. K.; Hartinger, C. G. Target Profiling of an Antimetastatic RAPTA Agent by Chemical Proteomics: Relevance to the Mode of Action. *Chem. Sci.* **2015**, *6* (4), 2449−2456.

(4) Murray, B. S.; Babak, M. V.; Hartinger, C. G.; Dyson, P. J. The Development of RAPTA Compounds for the Treatment of Tumors. *Coord. Chem. Rev.* **2016**, *306* (P1), 86−114.

(5) Mjos, K. D.; Orvig, C. Metallodrugs in Medicinal Inorganic Chemistry. *Chem. Rev.* **2014**, *114* (8), 4540−4563.

(6) Scolaro, C.; Bergamo, A.; Brescacin, L.; Delfino, R.; Cocchietto, M.; Laurenczy, G.; Geldbach, T. J.; Sava, G.; Dyson, P. J. In Vitro and in Vivo Evaluation of Ruthenium(II)-Arene PTA Complexes. *J. Med. Chem.* **2005**, *48* (12), 4161−4171.

(7) Englinger, B.; Pirker, C.; Heffeter, P.; Terenzi, A.; Kowol, C. R.; Keppler, B. K.; Berger, W. Metal Drugs and the Anticancer Immune Response. *Chem. Rev.* **2019**, *119* (2), 1519−1624.

(8) Rausch, M.; Dyson, P. J.; Nowak-Sliwinska, P. Recent Considerations in the Application of RAPTA-C for Cancer Treatment and Perspectives for Its Combination with Immunotherapies. *Adv. Ther.* **2019**, *2* (9), 1900042.

(9) Tremlett, W. D. J.; Goodman, D. M.; Steel, T. R.; Kumar, S.; Wieczorek-Błauż, A.; Walsh, F. P.; Sullivan, M. P.; Hanif, M.; Hartinger, C. G. Design Concepts of Half-Sandwich Organo-ruthenium Anticancer Agents Based on Bidentate Bioactive Ligands. *Coord. Chem. Rev.* **2021**, *445*, 213950.

(10) Honorato, J.; Oliveira, K.; Leite, C.; Colina-Vegas, L.; Nóbrega, J.; Castellano, E.; Ellena, J.; Correa, R.; Batista, A. Half-Sandwich/Ru^{II} Anticancer Complexes Containing Triphenylphosphine and p-

Substituted Benzoic Acids. *J. Braz. Chem. Soc.* **2020**, *31* (11). DOI: 10.21577/0103-5053.20200076.
(11) Kandioller, W.; Balsano, E.; Meier, S. M.; Jungwirth, U.; Göschl, S.; Roller, A.; Jakupec, M. A.; Berger, W.; Keppler, B. K.; Hartinger, C. G. Organometallic Anticancer Complexes of Lapachol: Metal Centre-Dependent Formation of Reactive Oxygen Species and Correlation with Cytotoxicity. *Chem. Commun.* **2013**, *49* (32), 3348.
(12) Tabrizi, L.; Chiniforoshan, H. Ruthenium(II) p-Cymene Complexes of Naphthoquinone Derivatives as Antitumor Agents: A Structure-activity Relationship Study. *J. Organomet. Chem.* **2016**, *822*, 211−220.
(13) Kubanik, M.; Tu, J. K. Y.; Söhnel, T.; Hejl, M.; Jakupec, M. A.; Kandioller, W.; Keppler, B. K.; Hartinger, C. G. Expanding on the Structural Diversity of Flavone-Derived RutheniumII(η^6-Arene) Anticancer Agents. *Metallodrugs* **2015**, *1* (1). DOI: 10.1515/medr-2015-0001.
(14) Kurzwernhart, A.; Kandioller, W.; Bartel, C.; Bächler, S.; Trondl, R.; Mühlgassner, G.; Jakupec, M. A.; Arion, V. B.; Marko, D.; Keppler, B. K.; Hartinger, C. G. Targeting the DNA-Topoisomerase Complex in a Double-Strike Approach with a Topoisomerase Inhibiting Moiety and Covalent DNA Binder. *Chem. Commun.* **2012**, *48* (40), 4839.
(15) Movassaghi, S.; Leung, E.; Hanif, M.; Lee, B. Y. T.; Holtkamp, H. U.; Tu, J. K. Y.; Söhnel, T.; Jamieson, S. M. F.; Hartinger, C. G. A Bioactive L-Phenylalanine-Derived Arene in Multitargeted Organo-ruthenium Compounds: Impact on the Antiproliferative Activity and Mode of Action. *Inorg. Chem.* **2018**, *57* (14), 8521−8529.
(16) Pettinari, R.; Marchetti, F.; Condello, F.; Pettinari, C.; Lupidi, G.; Scopelliti, R.; Mukhopadhyay, S.; Riedel, T.; Dyson, P. J. Ruthenium(II)-Arene RAPTA Type Complexes Containing Curcumin and Bisdemethoxycurcumin Display Potent and Selective Anticancer Activity. *Organometallics* **2014**, *33* (14), 3709−3715.
(17) Caruso, F.; Rossi, M.; Benson, A.; Opazo, C.; Freedman, D.; Monti, E.; Gariboldi, M. B.; Shaulky, J.; Marchetti, F.; Pettinari, R.; Pettinari, C. Ruthenium-Arene Complexes of Curcumin: X-Ray and Density Functional Theory Structure, Synthesis, and Spectroscopic Characterization, in Vitro Antitumor Activity, and DNA Docking Studies of (p -Cymene)Ru(Curcuminato)Chloro. *J. Med. Chem.* **2012**, *55* (3), 1072−1081.
(18) Huang, S.; Liang, Y.; Huang, C.; Su, W.; Lei, X.; Liu, Y.; Xiao, Q. Systematical Investigation of Binding Interaction between Novel Ruthenium(II) Arene Complex with Curcumin Analogs and CtDNA. *Luminescence* **2016**, *31* (7), 1384−1394.
(19) Bonfili, L.; Pettinari, R.; Cuccioloni, M.; Cecarini, V.; Mozzicafreddo, M.; Angeletti, M.; Lupidi, G.; Marchetti, F.; Pettinari, C.; Eleuteri, A. M. Arene-Ru II Complexes of Curcumin Exert Antitumor Activity via Proteasome Inhibition and Apoptosis Induction. *ChemMedChem.* **2012**, *7* (11), 2010−2020.
(20) Kubanik, M.; Kandioller, W.; Kim, K.; Anderson, R. F.; Klapproth, E.; Jakupec, M. A.; Roller, A.; Söhnel, T.; Keppler, B. K.; Hartinger, C. G. Towards Targeting Anticancer Drugs: Ruthenium-(II)-Arene Complexes with Biologically Active Naphthoquinone-Derived Ligand Systems. *Dalt. Trans.* **2016**, *45* (33), 13091−13103.
(21) Angelini, L. G.; Pistelli, L.; Belloni, P.; Bertoli, A.; Panconesi, S. Rubia Tinctorum a Source of Natural Dyes: Agronomic Evaluation, Quantitative Analysis of Alizarin and Industrial Assays. *Ind. Crops Prod.* **1997**, *6* (3−4), 303−311.
(22) Takahashi, E.; Fujita, K.; Kamataki, T.; Arimoto-Kobayashi, S.; Okamoto, K.; Negishi, T. Inhibition of Human Cytochrome P450 1B1, 1A1 and 1A2 by Antigenotoxic Compounds, Purpurin and Alizarin. *Mutat. Res. Mol. Mech. Mutagen.* **2002**, *508* (1−2), 147−156.
(23) Fotia, C.; Avnet, S.; Granchi, D.; Baldini, N. The Natural Compound Alizarin as an Osteotropic Drug for the Treatment of Bone Tumors. *J. Orthop. Res.* **2012**, *30* (9), 1486−1492.
(24) Jäger, I.; Hafner, C.; Welsch, C.; Schneider, K.; Iznaguen, H.; Westendorf, J. The Mutagenic Potential of Madder Root in Dyeing Processes in the Textile Industry. *Mutat. Res. Toxicol. Environ. Mutagen.* **2006**, *605* (1−2), 22−29.
(25) Wölfle, D.; Schmutte, C.; Westendorf, J.; Marquardt, H. Hydroxyanthraquinones as Tumor Promoters: Enhancement of Malignant Transformation of C3H Mouse Fibroblasts and Growth Stimulation of Primary Rat Hepatocytes. *Cancer Res.* **1990**, *50* (20), 6540−6544.
(26) Xie, X.; Ross, J. L.; Cowell, J. K.; Teng, Y. The Promise of Zebrafish as a Chemical Screening Tool in Cancer Therapy. *Future Med. Chem.* **2015**, *7* (11), 1395−1405.
(27) Trigueiro, N. S. de S.; Canedo, A.; Braga, D. L. de S.; Luchiari, A. C.; Rocha, T. L. Zebrafish as an Emerging Model System in the Global South: Two Decades of Research in Brazil. *Zebrafish* **2020**, *17* (6), 412−425.
(28) Brundo, M. V.; Salvaggio, A. Zebrafish or Danio Rerio: A New Model in Nanotoxicology Study. *Recent Advances in Zebrafish Researches*; InTech, 2018. DOI: 10.5772/intechopen.74834.
(29) Stuelten, C. H.; Parent, C. A.; Montell, D. J. Cell Motility in Cancer Invasion and Metastasis: Insights from Simple Model Organisms. *Nat. Rev. Cancer* **2018**, *18* (5), 296−312.
(30) Barbazuk, W. B.; Korf, I.; Kadavi, C.; Heyen, J.; Tate, S.; Wun, E.; Bedell, J. A.; McPherson, J. D.; Johnson, S. L. The Syntenic Relationship of the Zebrafish and Human Genomes. *Genome Res.* **2000**, *10* (9), 1351−1358.
(31) Huszno, J.; Klag, J. The Reproductive Cycle in the Male Gonads of Danio Rerio (Teleostei, Cyprinidae). Stereological Analysis. *Micron* **2012**, *43* (5), 666−672.
(32) Fukushima, H. C. S.; Bailone, R. L.; Corrêa, T.; Janke, H.; De Aguiar, L. K.; Setti, P. G.; Borra, R. C. Zebrafish Toxicological Screening Could Aid Leishmaniosis Drug Discovery. *Lab. Anim. Res.* **2021**, *37* (1), 27.
(33) Batista-Filho, J.; Falcão, M. A. P.; Maleski, A. L. A.; Soares, A. B. S.; Balan-Lima, L.; Disner, G. R.; Lima, C.; Lopes-Ferreira, M. Early Preclinical Screening Using Zebrafish (Danio Rerio) Reveals the Safety of the Candidate Anti-Inflammatory Therapeutic Agent TnP. *Toxicol. Reports* **2021**, *8*, 13−22.
(34) Lee, K. Y.; Jang, G. H.; Byun, C. H.; Jeun, M.; Searson, P. C.; Lee, K. H. Zebrafish Models for Functional and Toxicological Screening of Nanoscale Drug Delivery Systems: Promoting Preclinical Applications. *Biosci. Rep.* **2017**, *37* (3). DOI: 10.1042/BSR20170199.
(35) Canedo, A.; Saiki, P.; Santos, A. L.; Carneiro, K. da S.; Souza, A. M. de; Qualhato, G.; Brito, R. da S.; Mello-Andrade, F.; Rocha, T. L. Zebrafish (Danio Rerio) Meets Bioethics: The 10Rs Ethical Principles in Research. *Ciência Anim. Bras.* **2022**, *23*. DOI: 10.1590/1809-6891v22e-70884.
(36) Zelonka, R. A.; Baird, M. C. Benzene Complexes of Ruthenium(II). *Can. J. Chem.* **1972**, *50* (18), 3063−3072.
(37) Serron, S. A.; Nolan, S. P. Enthalpies of Reaction of ((p-Cymene)RuCl2)2 with Monodentate Tertiary Phosphine Ligands. Importance of Both Steric and Electronic Ligand Factors in a Ruthenium(II) System. *Organometallics* **1995**, *14* (10), 4611−4616.
(38) Pertici, P.; Bertozzi, S.; Lazzaroni, R.; Vitulli, G.; Bennett, M. A. A Simple Method of Regenerating Areneruthenium Dichloride Dimers, [RuCl2(H6-Arene)]2, from Their Monomeric Adducts with Amines or Tertiary Phosphines, RuCl2(H6-Arene)L. *J. Organomet. Chem.* **1988**, *354* (1), 117−121.
(39) Menye-Biyogo, R.; Delpech, F.; Castel, A.; Gornitzka, H.; Rivière, P. Ruthenium-Stabilized Low-Coordinate Phosphorus Atoms: Structural Evidence for Monomeric Metaphosphonate. *Angew. Chemie Int. Ed.* **2003**, *42* (45), 5610−5612.
(40) Graminha, A. E.; Honorato, J.; Dulcey, L. L.; Godoy, L. R.; Barbosa, M. F.; Cominetti, M. R.; Menezes, A. C.; Batista, A. A. Evaluation of the Biological Potential of Ruthenium(II) Complexes with Cinnamic Acid. *J. Inorg. Biochem.* **2020**, *206*, 111021.
(41) Cyrański, M. K.; Jamróz, M. H.; Rygula, A.; Dobrowolski, J. C.; Dobrzycki, Ł.; Baranska, M. On Two Alizarin Polymorphs. *CrystEngComm* **2012**, *14* (10), 3667.
(42) Rahman, D. S.; Chatterjee, H.; Ghosh, S. K. Excess Surface Energy at the Tips of Gold Nanospikes: From Experiment to Modeling. *J. Phys. Chem. C* **2015**, *119* (25), 14326−14337.

https://doi.org/10.1021/acs.inorgchem.3c00183
Inorg. Chem. 2023, 62, 6955−6969

(43) Vaughan, J. C.; Dempsey, G. T.; Sun, E.; Zhuang, X. Phosphine Quenching of Cyanine Dyes as a Versatile Tool for Fluorescence Microscopy. *J. Am. Chem. Soc.* **2013**, *135* (4), 1197−1200.
(44) Mackenzie, H. K.; Rawe, B. W.; Samedov, K.; Walsgrove, H. T. G.; Uva, A.; Han, Z.; Gates, D. P. A Smart Phosphine-Diyne Polymer Displays "Turn-On" Emission with a High Selectivity for Gold(I/III) Ions. *J. Am. Chem. Soc.* **2020**, *142* (23), 10319−10324.
(45) Wood, P. A.; Olsson, T. S. G.; Cole, J. C.; Cottrell, S. J.; Feeder, N.; Galek, P. T. A.; Groom, C. R.; Pidcock, E. Evaluation of Molecular Crystal Structures Using Full Interaction Maps. *CrystEngComm* **2013**, *15* (1), 65−72.
(46) Macrae, C. F.; Sovago, I.; Cottrell, S. J.; Galek, P. T. A.; McCabe, P.; Pidcock, E.; Platings, M.; Shields, G. P.; Stevens, J. S.; Towler, M.; Wood, P. A. Mercury 4.0 : From Visualization to Analysis, Design and Prediction. *J. Appl. Crystallogr.* **2020**, *53* (1), 226−235.
(47) Gossens, C.; Tavernelli, I.; Rothlisberger, U. DNA Structural Distortions Induced by Ruthenium-Arene Anticancer Compounds. *J. Am. Chem. Soc.* **2008**, *130* (33), 10921−10928.
(48) Jeyalakshmi, K.; Haribabu, J.; Balachandran, C.; Swaminathan, S.; Bhuvanesh, N. S. P.; Karvembu, R. Coordination Behavior of N,N′,N″-Trisubstituted Guanidine Ligands in Their Ru-Arene Complexes: Synthetic, DNA/Protein Binding, and Cytotoxic Studies. *Organometallics* **2019**, *38* (4), 753.
(49) Biancalana, L.; Pampaloni, G.; Zacchini, S.; Marchetti, F. Synthesis, Characterization and Behavior in Water/DMSO Solution of Ru(II) Arene Complexes with Bioactive Carboxylates. *J. Organomet. Chem.* **2018**, *869*, 201−211.
(50) Crul, M.; van Waardenburg, R. C. A.; Beijnen, J.; Schellens, J. H. DNA-Based Drug Interactions of Cisplatin. *Cancer Treat. Rev.* **2002**, *28* (6), 291−303.
(51) Gonzalez, V. M.; Fuertes, M. A.; Alonso, C.; Perez, J. M. Is Cisplatin-Induced Cell Death Always Produced by Apoptosis? *Mol. Pharmacol.* **2001**, *59* (4), 657−663.
(52) Alsaeedi, M. S.; Babgi, B. A.; Abdellattif, M. H.; Jedidi, A.; Humphrey, M. G.; Hussien, M. A. DNA-Binding Capabilities and Anticancer Activities of Ruthenium(II) Cymene Complexes with (Poly)Cyclic Aromatic Diamine Ligands. *Molecules* **2021**, *26* (1), 76.
(53) Sathiya Kamatchi, T.; Chitrapriya, N.; Kim, S. K.; Fronczek, F. R.; Natarajan, K. Influence of Carboxylic Acid Functionalities in Ruthenium (II) Polypyridyl Complexes on DNA Binding, Cytotoxicity and Antioxidant Activity: Synthesis, Structure and in Vitro Anticancer Activity. *Eur. J. Med. Chem.* **2013**, *59*, 253−264.
(54) Colina-Vegas, L.; Luna-Dulcey, L.; Plutín, A. M.; Castellano, E. E.; Cominetti, M. R.; Batista, A. A. Half Sandwich Ru(II)-Acylthiourea Complexes: DNA/HSA-Binding, Anti-Migration and Cell Death in a Human Breast Tumor Cell Line. *Dalt. Trans.* **2017**, *46* (38), 12865−12875.
(55) Honorato, J.; Colina-Vegas, L.; Correa, R. S.; Guedes, A. P. M. M.; Miyata, M.; Pavan, F. R.; Ellena, J.; Batista, A. A. Esterification of the Free Carboxylic Group from the Lutidinic Acid Ligand as a Tool to Improve the Cytotoxicity of Ru(II) Complexes. *Inorg. Chem. Front.* **2019**, *6* (2), 376−390.
(56) Gkionis, K.; Platts, J. A.; Hill, J. G. Insights into DNA Binding of Ruthenium Arene Complexes: Role of Hydrogen Bonding and π Stacking. *Inorg. Chem.* **2008**, *47* (9), 3893−3902.
(57) Novakova, O.; Chen, H.; Vrana, O.; Rodger, A.; Sadler, P. J.; Brabec, V. DNA Interactions of Monofunctional Organometallic Ruthenium(II) Antitumor Complexes in Cell-Free Media. *Biochemistry* **2003**, *42* (39), 11544−11554.
(58) Graminha, A. E.; Honorato, J.; Correa, R. S.; Cominetti, M. R.; Menezes, A. C. S.; Batista, A. A. A Novel Ruthenium(II) Gallic Acid Complex Disrupts the Actin Cytoskeleton and Inhibits Migration, Invasion and Adhesion of Triple Negative Breast Tumor Cells. *Dalt. Trans.* **2021**, *50* (1), 323−335.
(59) Iqbal, S.; Siddiqui, W. A.; Ashraf, A.; Tong, K. K. H.; Aman, F.; Söhnel, T.; Jamieson, S. M. F.; Hanif, M.; Hartinger, C. G. Substitution of the Chlorido Ligand for PPh3 in Anticancer Organoruthenium Complexes of Sulfonamide-Functionalized Pyridine-2-Carbothioamides Leads to High Cytotoxic Activity. *Inorg. Chim. Acta* **2022**, *536*, 120889.
(60) McKeage, M. J.; Berners-Price, S. J.; Galettis, P.; Bowen, R. J.; Brouwer, W.; Ding, L.; Zhuang, L.; Baguley, B. C. Role of Lipophilicity in Determining Cellular Uptake and Antitumour Activity of Gold Phosphine Complexes. *Cancer Chemother. Pharmacol.* **2000**, *46* (5), 343−350.
(61) Franken, N. A. P.; Rodermond, H. M.; Stap, J.; Haveman, J.; van Bree, C. Clonogenic Assay of Cells in Vitro. *Nat. Protoc.* **2006**, *1* (5), 2315−2319.
(62) Munshi, A.; Hobbs, M.; Meyn, R. E. Clonogenic Cell Survival Assay. *Chemosensitivity*; Humana Press: Totowa, NJ, 2005; pp 021−028. DOI: 10.1385/1-59259-869-2:021.
(63) Allardyce, C. S.; Dyson, P. J. Metal-Based Drugs That Break the Rules. *Dalt. Trans.* **2016**, *45* (8), 3201−3209.
(64) Scolaro, C.; Bergamo, A.; Brescacin, L.; Delfino, R.; Cocchietto, M.; Laurenczy, G.; Geldbach, T. J.; Sava, G.; Dyson, P. J. In Vitro and in Vivo Evaluation of Ruthenium(II)-Arene PTA Complexes. *J. Med. Chem.* **2005**, *48* (12), 4161−4171.
(65) Sonkar, C.; Sarkar, S.; Mukhopadhyay, S. Ruthenium(II)-Arene Complexes as Anti-Metastatic Agents, and Related Techniques. *RSC Med. Chem.* **2022**, *13* (1), 22−38.
(66) Khodjakov, A.; Rieder, C. L. The Nature of Cell-Cycle Checkpoints: Facts and Fallacies. *J. Biol.* **2009**, *8* (10), 88.
(67) Cabrera, M.; Gomez, N.; Remes Lenicov, F.; Echeverría, E.; Shayo, C.; Moglioni, A.; Fernández, N.; Davio, C. G2/M Cell Cycle Arrest and Tumor Selective Apoptosis of Acute Leukemia Cells by a Promising Benzophenone Thiosemicarbazone Compound. *PLoS One* **2015**, *10* (9), No. e0136878.
(68) Malumbres, M.; Barbacid, M. Cell Cycle, CDKs and Cancer: A Changing Paradigm. *Nat. Rev. Cancer* **2009**, *9* (3), 153−166.
(69) Pan, Z.; Zhang, X.; Yu, P.; Chen, X.; Lu, P.; Li, M.; Liu, X.; Li, Z.; Wei, F.; Wang, K.; Zheng, Q.; Li, D. Cinobufagin Induces Cell Cycle Arrest at the G2/M Phase and Promotes Apoptosis in Malignant Melanoma Cells. *Front. Oncol.* **2019**, *9*, 853.
(70) Huang, X.; Halicka, H. D.; Traganos, F.; Tanaka, T.; Kurose, A.; Darzynkiewicz, Z. Cytometric Assessment of DNA Damage in Relation to Cell Cycle Phase and Apoptosis. *Cell Prolif.* **2005**, *38* (4), 223−243.
(71) Teixeira, T. M.; Arraes, I. G.; Abreu, D. C.; Oliveira, K. M.; Correa, R. S.; Batista, A. A.; Braunbeck, T.; de Paula Silveira Lacerda, E. Ruthenium Complexes Show Promise When Submitted to Toxicological Safety Tests Using Alternative Methodologies. *Eur. J. Med. Chem.* **2021**, *216*, 113262.
(72) Golbaghi, G.; Pitard, I.; Lucas, M.; Haghdoost, M. M.; de los Santos, Y. L.; Doucet, N.; Patten, S. A.; Sanderson, J. T.; Castonguay, A. Synthesis and Biological Assessment of a Ruthenium(II) Cyclopentadienyl Complex in Breast Cancer Cells and on the Development of Zebrafish Embryos. *Eur. J. Med. Chem.* **2020**, *188*, 112030.
(73) Velozo-Sá, V. S.; Pereira, L. R.; Lima, A. P.; Mello-Andrade, F.; Rezende, M. R. M.; Goveia, R. M.; Pires, W. C.; Silva, M. M.; Oliveira, K. M.; Ferreira, A. G.; Ellena, J.; Deflon, V. M.; Grisolia, C. K.; Batista, A. A.; Silveira-Lacerda, E. P. In Vitro Cytotoxicity and in Vivo Zebrafish Toxicity Evaluation of Ru(II)/2-Mercaptopyrimidine Complexes. *Dalt. Trans.* **2019**, *48* (18), 6026−6039.
(74) Mello-Andrade, F.; Cardoso, C. G.; Silva, C. R. e; Chen-Chen, L.; Melo-Reis, P. R. de; Lima, A. P. de; Oliveira, R.; Ferraz, I. B. M.; Grisolia, C. K.; Almeida, M. A. P.; Batista, A. A.; Silveira-Lacerda, E. de P. Acute Toxic Effects of Ruthenium (II)/Amino Acid/Diphosphine Complexes on Swiss Mice and Zebrafish Embryos. *Biomed. Pharmacother.* **2018**, *107*, 1082−1092.
(75) Lenis-Rojas, O. A.; Roma-Rodrigues, C.; Fernandes, A. R.; Marques, F.; Pérez-Fernández, D.; Guerra-Varela, J.; Sánchez, L.; Vázquez-García, D.; López-Torres, M.; Fernández, A.; Fernández, J. J. Dinuclear RuII(Bipy)2 Derivatives: Structural, Biological, and in Vivo Zebrafish Toxicity Evaluation. *Inorg. Chem.* **2017**, *56* (12), 7127−7144.

https://doi.org/10.1021/acs.inorgchem.3c00183
Inorg. Chem. 2023, 62, 6955−6969

(76) Haghdoost, M.; Golbaghi, G.; Létourneau, M.; Patten, S. A.; Castonguay, A. Lipophilicity-Antiproliferative Activity Relationship Study Leads to the Preparation of a Ruthenium(II) Arene Complex with Considerable in Vitro Cytotoxicity against Cancer Cells and a Lower in Vivo Toxicity in Zebrafish Embryos than Clinically Approved C. *Eur. J. Med. Chem.* **2017**, *132*, 282−293.
(77) Wu, Q.; Zheng, K.; Liao, S.; Ding, Y.; Li, Y.; Mei, W. Arene Ruthenium(II) Complexes as Low-Toxicity Inhibitor against the Proliferation, Migration, and Invasion of MDA-MB-231 Cells through Binding and Stabilizing c-Myc G-Quadruplex DNA. *Organometallics* **2016**, *35* (3), 317−326.
(78) von Hellfeld, R.; Brotzmann, K.; Baumann, L.; Strecker, R.; Braunbeck, T. Adverse Effects in the Fish Embryo Acute Toxicity (FET) Test: A Catalogue of Unspecific Morphological Changes versus More Specific Effects in Zebrafish (Danio Rerio) Embryos. *Environ. Sci. Eur.* **2020**, *32* (1), 122.
(79) Sant, K. E.; Timme-Laragy, A. R. Zebrafish as a Model for Toxicological Perturbation of Yolk and Nutrition in the Early Embryo. *Curr. Environ. Heal. Reports* **2018**, *5* (1), 125−133.
(80) Hill, A. J. Water Permeability and TCDD-Induced Edema in Zebrafish Early-Life Stages. *Toxicol. Sci.* **2004**, *78* (1), 78−87.
(81) Kimmel, C. B.; Ballard, W. W.; Kimmel, S. R.; Ullmann, B.; Schilling, T. F. Stages of Embryonic Development of the Zebrafish. *Dev. Dyn.* **1995**, *203* (3), 253−310.
(82) Novokmet, S.; Stojic, I.; Radonjic, K.; Savic, M.; Jeremic, J. Toxic Effects of Metallopharmaceuticals. *Serbian J. Exp. Clin. Res.* **2017**, *18* (3), 191−194.
(83) Santoso, F.; Farhan, A.; Castillo, A. L.; Malhotra, N.; Saputra, F.; Kurnia, K. A.; Chen, K. H.-C.; Huang, J.-C.; Chen, J.-R.; Hsiao, C.-D. An Overview of Methods for Cardiac Rhythm Detection in Zebrafish. *Biomedicines* **2020**, *8* (9), 329.

https://doi.org/10.1021/acs.inorgchem.3c00183
Inorg. Chem. 2023, 62, 6955−6969